ELSEVIER

PII: S0032-3861(97)00346-7

Polymer Vol. 39 No. 4, pp. 781–792, 1998

0032-3861/97/$17.00+0.00

Time resolved simultaneous small- and wide-angle X-ray scattering during polyethylene deformation 3. Compression of polyethylene

Michael F. Butler[a,†], Athene M. Donald[a,*,†] and Anthony J. Ryan[b,c]
[a]*Department of Physics, Cavendish Laboratory, University of Cambridge, Madingley Road, Cambridge CB3 0HE, UK*
[b]*CCLRC Daresbury Laboratory, Daresbury, Warrington, Cheshire WA4 4AD, UK*
[c]*Materials Science Centre, UMIST, Grosvenor Street, Manchester M1 7HS, UK*
(Received 20 December 1996; revised 10 March 1997)

The compression behaviour of a range of unoriented linear and branched polyethylenes was investigated using the technique of simultaneous small- and wide-angle X-ray scattering during deformation. Interlamellar deformation mechanisms, including simultaneous shear and rotation of lamellar stacks, were followed by crystallographic deformation mechanisms, including (100)[001] chain slip and a martensitic transformation. Immediate post-yield deformation behaviour involved a reconstruction of the lamellar microstructure, the deformation of which was responsible for strain hardening. The reconstruction process, which involved extensive lamellar rearrangement, was aided by the increased amount of amorphous material in the less crystalline linear low density branched polyethylenes. Branch length, however, was found to be unimportant. © 1997 Elsevier Science Ltd.

(Keywords: X-ray scattering; polyethylene; compression)

INTRODUCTION

This paper is the third in a series of three reporting the findings from an investigation into the micromechanical behaviour of commercial grade polyethylenes (PE) deformed at room temperature. The first two papers[1,2] reported the tensile properties of a range of ethylene–α-olefin copolymers and linear polyethylenes respectively, using the technique of time-resolved simultaneous measurement of the small- and wide-angle X-ray scattering patterns (SAXS and WAXS respectively) and macroscopic deformation using high intensity synchrotron radiation. Due to the success of the tensile experiments[1–3], in which the elimination of sample relaxation enabled by a real-time *in-situ* study revealed a variety of correlations between macroscopic, lamellar and molecular deformation, the technique was extended to a study of the compressive behaviour.

One of the motivations for studying compressive deformation is the absence of voiding in HDPE during compression at room temperature, allowing lamellar deformation to be followed over the whole deformation range via SAXS (the large density difference between amorphous PE and void is the cause of the high intensity of the void scattering in cold-drawn HDPE[4], which completely overwhelms the lamellar scattering[1,3]) Despite this, only a few compression studies on unoriented HDPE have been reported[5–7]. However, a substantial body of work exists on single crystal textured oriented PE, performed in order to study the individual deformation mechanisms. Many have been identified in compression, including lamellar eparation, rotation and shear, chain and transverse slip, deformation twinning and a stress-induced martensitic transformation[8–15]. Although some studies have been performed *in situ*, in order to overcome the substantial problem of relaxation[5,11,12,16], it is believed that the work presented in this paper forms the first time-resolved X-ray scattering study during compression of PE.

A model was proposed by Peterlin to account for the lamellar to fibrillar transformation that occurs during the drawing of PE[17]. The mechanism is still uncertain, however, and there is some debate on whether crystallographic deformation proceeds via nucleation and glide of dislocations in the lamellae[18–21], or whether a partial melting and recrystallisation process occurs[22–28]. A model explaining the structural changes in compression was proposed by Galeski *et al.*[6]. Lamellae initially rotate and shear on the (100)[001] slip system until they have reached approximately one third of their initial thickness. Deformation of the accompanying amorphous material renders the chain slip that occurs as the lamellae shear unstable, and they break up in the process referred to as 'coarse slip'[14]. The lamellar fragments can then rotate without constraint so that the chains align with the flow direction. The process is a continuous one.

EXPERIMENTAL

A range of linear polyethylenes and ethylene–α-olefin copolymers, supplied by BP Chemicals Ltd., were studied in uniaxial compression. *Table 1* shows details of the samples used (which were the same as those studied in tension in previous publications[1–3]). They formed a range of polyethylenes with different molecular weights ($60\,000 \leq M_W \leq 385\,000$) and branch types. Compression specimens

* To whom correspondence should be addressed.
† Tel: (+ 44) (0)1223 337007. Fax: (+ 44) (0)1223 337000.

Table 1 Sample information

Sample	M_w/1000	M_w/M_n	Branch amount per 1000C	Percentage crystallinity	Lamellar thickness (nm)
A	60	4.7	< 2.0	70.2 ± 0.3	24.0 ± 2.1
B	131	6.3	< 0.5	70.0 ± 0.6	28.1 ± 2.4
E (unannealed)	385	9.0	0	65.5 ± 0.9	27.3 ± 2.4
E (annealed)	385	9.0	0	74.4 ± 0.1	45.0 ± 3.9
G (unannealed)	152	5.2	23.7	35.8 ± 0.1	12.7 ± 1.1
G (annealed)	152	5.2	23.7	39.5 ± 1.0	13.3 ± 1.2
H (unannealed)	126	4.2	21.0	39.0 ± 0.4	14.4 ± 1.2
H (annealed)	126	4.2	21.0	43.8 ± 0.4	14.8 ± 1.3
I	110	3.0	~20	34.4 ± 0.4	14.3 ± 1.2

The percentage crystallinities and lamellar thicknesses were obtained from DSC[1-3]. All samples were studied unannealed. Annealed specimens of samples E, G and H were also studied.

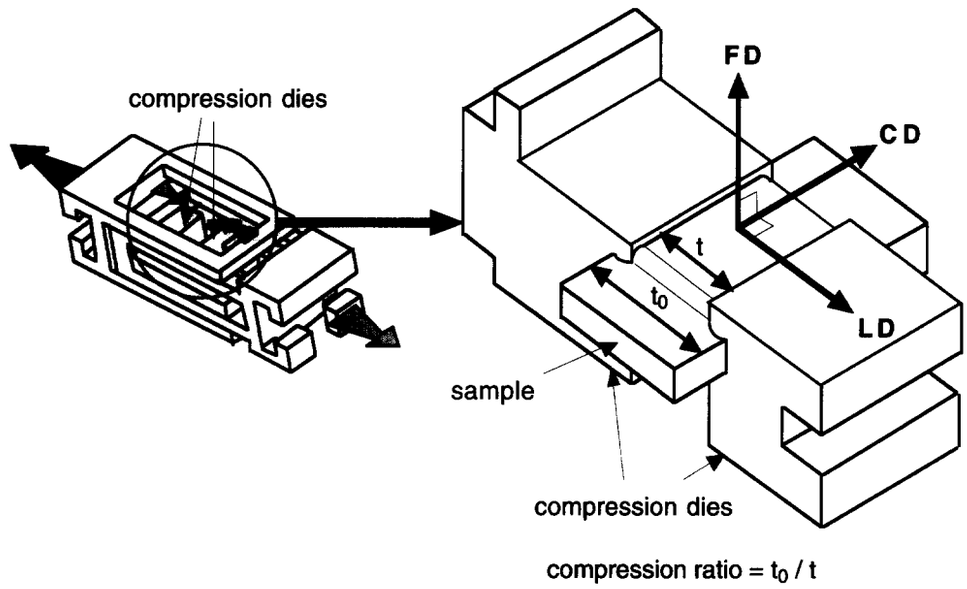

Figure 1 Schematic diagram of the compression apparatus which was used for the time-resolved *in-situ* compression experiments, with the compression dies and deformation geometry detailed. The large flat top surfaces of the dies were made so that they did not impede the WAXS

2.5 mm wide and 30 mm long were cut from plaques 0.9 mm thick (details of the production of the plaques has been given previously[1-3]). They were compressed uniformly along their length, parallel to their width, from the initial width of 2.5 mm, chosen to ensure that the samples compressed rather than buckled, to a final one of approximately 0.5 mm. A specially constructed compression device mounted in a Rheometrics Limited Miniature Materials Tester (Minimat) was used. Further details of the construction of this device can be found elsewhere[29]. *Figure 1* shows a simplified view of the compression dies, demonstrating how it was possible to measure the WAXS and SAXS simultaneously during compression and indicating the deformation geometry. The compressive axis is defined as LD, the load direction. The flow direction of the sample is defined as FD, and was parallel to the incident X-ray beam. The direction mutually perpendicular to LD and FD is defined as CD, the constraint direction, in which no macroscopic movement of the sample occurred.

All of the samples were compressed at room temperature, at a nominal compression rate of 0.5 mm min^{-1}. A few specimens were compressed at 0.05 and 5.0 mm min^{-1}, to study the influence of compression rate on the deformation mechanisms. SAXS and WAXS patterns and the load–compression curve were measured simultaneously during compression using the experimental set-up and detectors described and illustrated previously[1,3], on beamlines 2.1 and 16.1 at the Synchrotron Radiation Source, Daresbury, UK[30-32]. The complete WAXS pattern was constructed by measuring the WAXS patterns from separate samples with the Minimat mounted both vertically and horizontally.

Measurements of sample dimensions were possible for some samples after compression and unloading, which allowed the load–extension curve to be converted to a

stress–strain curve by assuming that the deformation had occurred at a constant compression rate and at constant volume. The strain was measured in terms of the compression ratio, which was the ratio between the initial thickness and the thickness of the samples at some point during deformation.

RESULTS

Macroscopic deformation

In all cases the load–compression curves displayed three distinct regimes: an initial elastic deformation, a yielding region, where the rate of increase of applied load decreased, and strain hardening. Unlike the case for tensile deformation at room temperature, a clear and distinct yield point (load maximum) was not observed during compression. Therefore the transition between elastic and plastic deformation and the onset of yielding could not be identified with certainty from the load–compression curves. However, conversion of the data, where possible, into a stress–strain curve showed a definite yield point (stress maximum) followed by strain softening before strain hardening commenced, which proved to be more useful in correlating the structural information revealed by SAXS and WAXS. *Figure 2* compares the load–extension and stress–strain curves for untreated B.

It should be noted that conversion of the load–extension curve to a stress–strain curve was fraught with possible sources of error. Firstly, the values of compression reported by the Minimat were patently incorrect. For example, sample B was compressed from an initial thickness of 2.00 mm to a final one of 0.36 mm (measured after unloading), yet the Minimat registered a compression of 2.00 mm. The actual displacement measured depended very much upon the modulus of the PE sample, and it is likely that the compression rate was not uniform throughout deformation. Secondly, relaxation of the samples after unloading introduced an uncertainty into the value of the sample thickness at the end of deformation. Relaxation of compressed samples has been found to be quite substantial in the first few minutes after deformation[5]. The results for the HDPE were treated as more reliable, since relaxation occurred to a lesser extent in these samples. These facts are mentioned here in order to highlight the difficulty in comparing different samples, e.g. in comparing the strains at

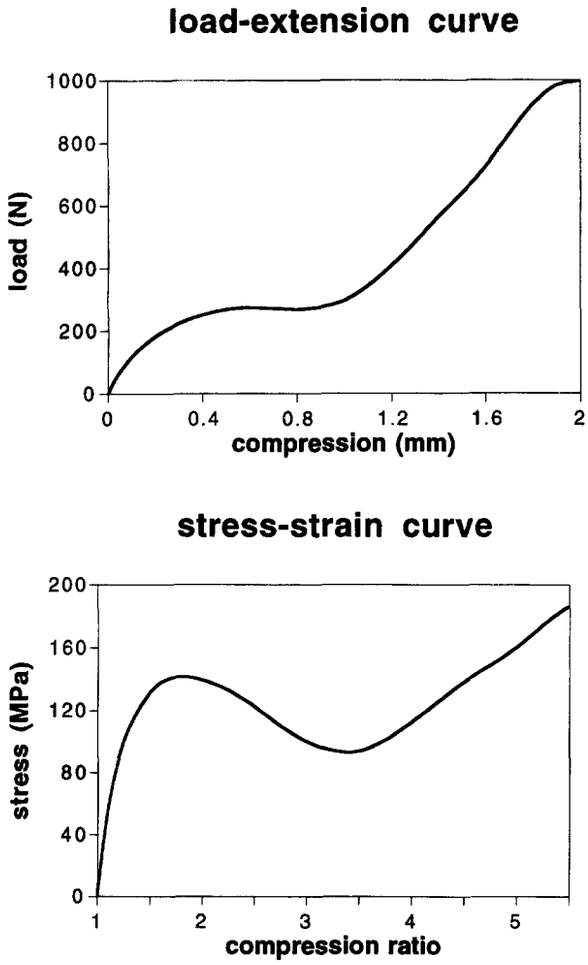

Figure 2 Comparison of the stress–strain curve and the load–extension curve from which it was derived for HDPE sample B deformed in compression

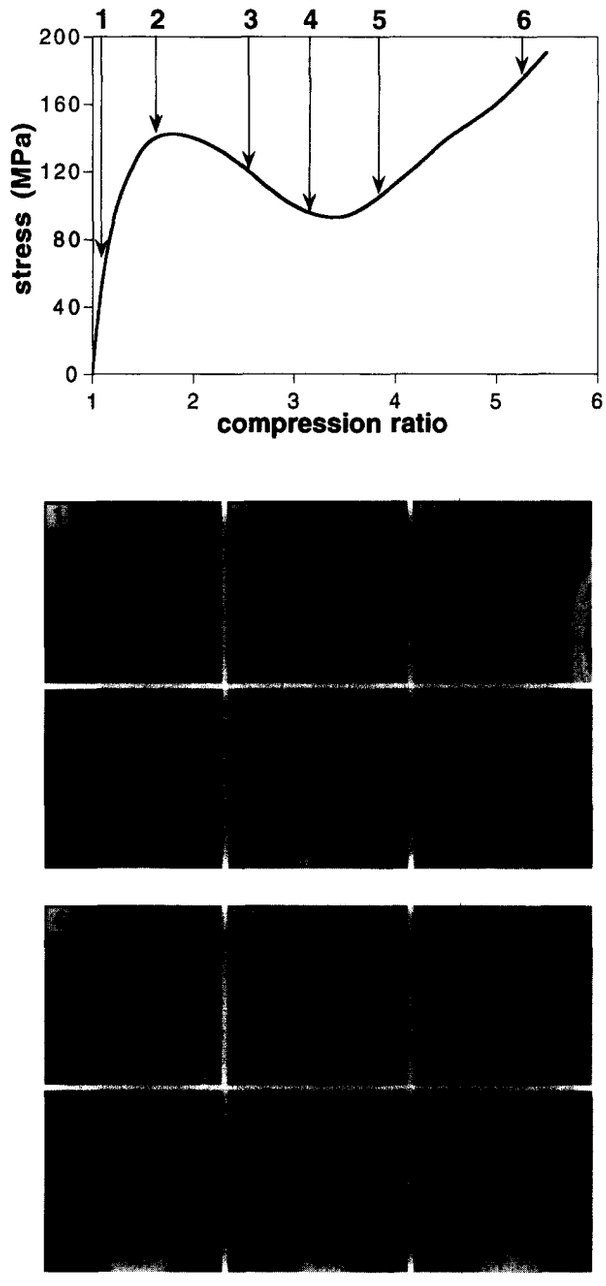

Figure 3 (a) Simultaneously obtained SAXS and partial WAXS (parallel to CD) patterns and (b) stress–strain curve for compressed HDPE sample B. The compressive axis is indicated, as is the monoclinic (001) reflection that appeared at the yield point

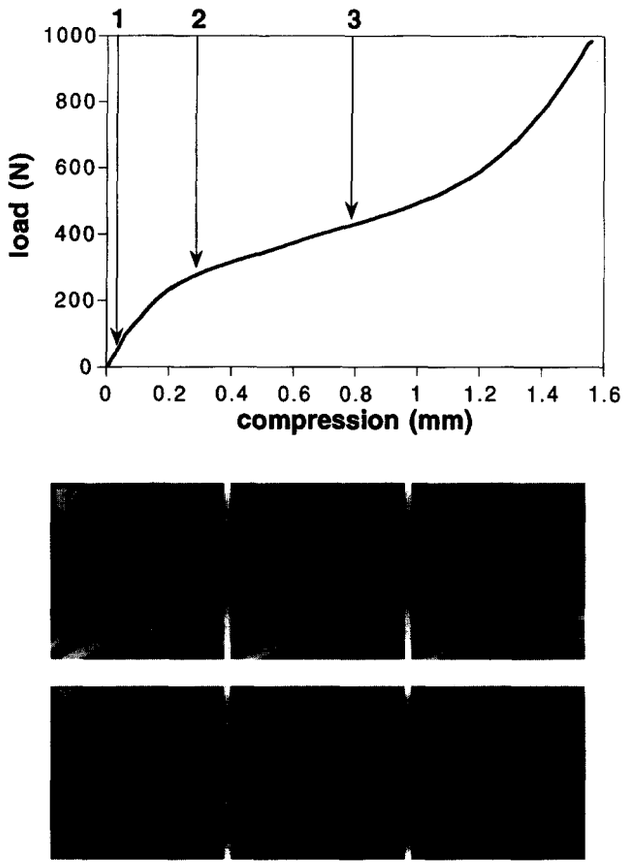

Figure 4 (a) Simultaneously obtained SAXS and partial WAXS (parallel to LD) patterns and (b) load–compression curve for compressed HDPE sample B. The compressive axis and stress-induced monoclinic (020) and ($\bar{2}$ 01) reflections are indicated

which the martensitic transformation or chain slip occurred for different samples.

For the samples deformed at different compression rates the yield stress increased with increasing compression rate, whereas the yield strain followed the opposite trend.

Wide-angle X-ray scattering

The WAXS patterns evolved similarly during compression for HDPE and LLDPE. *Figures 3 and 4* show the SAXS and WAXS patterns and the simultaneously obtained load–compression curves for untreated B with LD horizontal and vertical respectively. SAXS and WAXS patterns were not obtained over the whole deformation range in the latter case because of experimental constraints. Owing to experimental constraints, the larger size and lower intensity of the beam on the samples for which the WAXS parallel to LD was measured caused the compression dies to obstruct the incident beam after a certain amount of compression. *Figure 5* shows the scattering patterns (WAXS parallel to CD) and load–compression curve for an LLDPE, untreated G. The evolution of the WAXS intensities parallel to CD during compression is shown in *Figure 6* for annealed E. *Figures 7 and 8* show the correlation between the WAXS intensities parallel to CD, SAXS long spacings and load–compression curves for the untreated linear PE and copolymer samples respectively. *Figure 9* illustrates the correlations much more effectively using the stress–strain curve instead of the load–compression curve for the HDPE samples A and B and the HMW-HDPE sample E.

With the exception of EU, no change was observed for

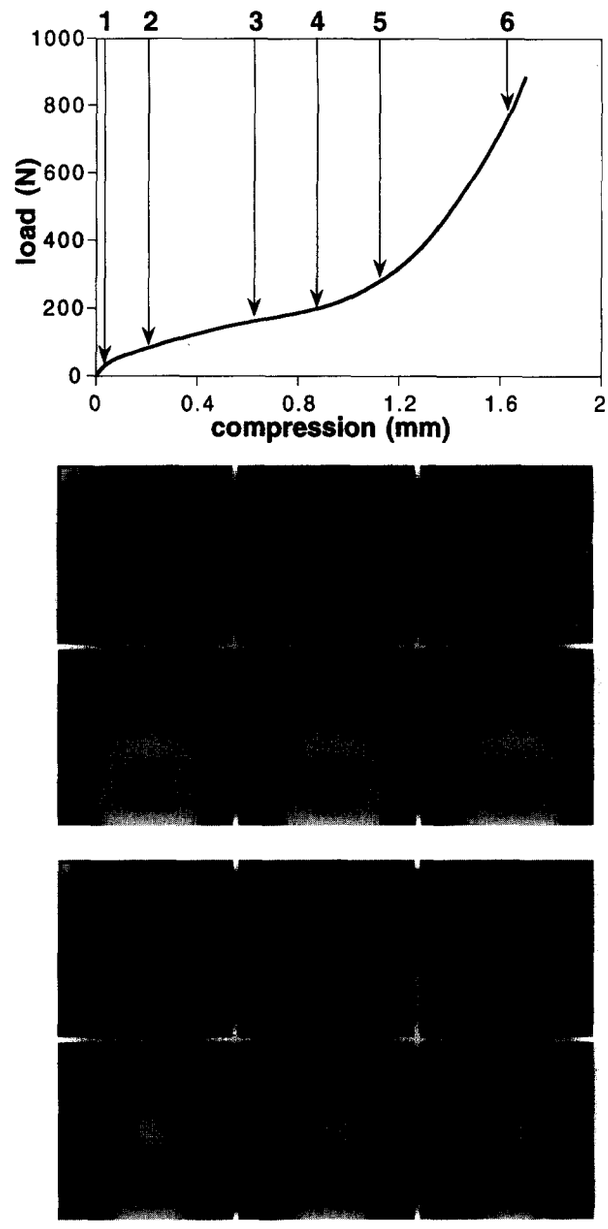

Figure 5 (a) Simultaneously obtained SAXS and partial WAXS (parallel to CD) patterns and (b) stress–strain curve for compressed LLDPE sample H. Note the difference in SAXS from the HDPE. The compressive axis is indicated

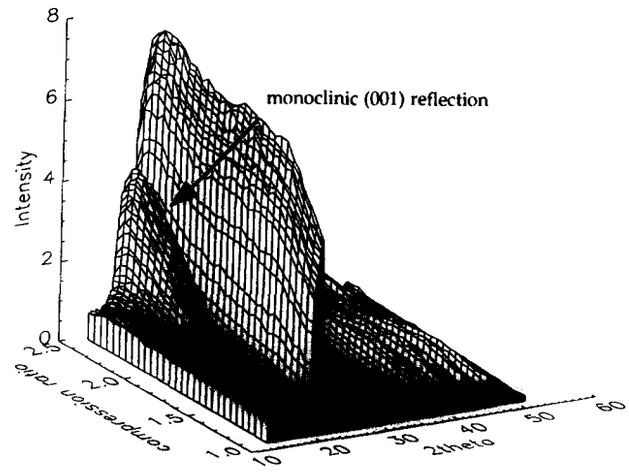

Figure 6 Evolution of the WAXS intensities parallel to CD for annealed HMW-HDPE sample E. The increase in intensity of the monoclinic (001) reflection, which is arrowed, is clearly visible

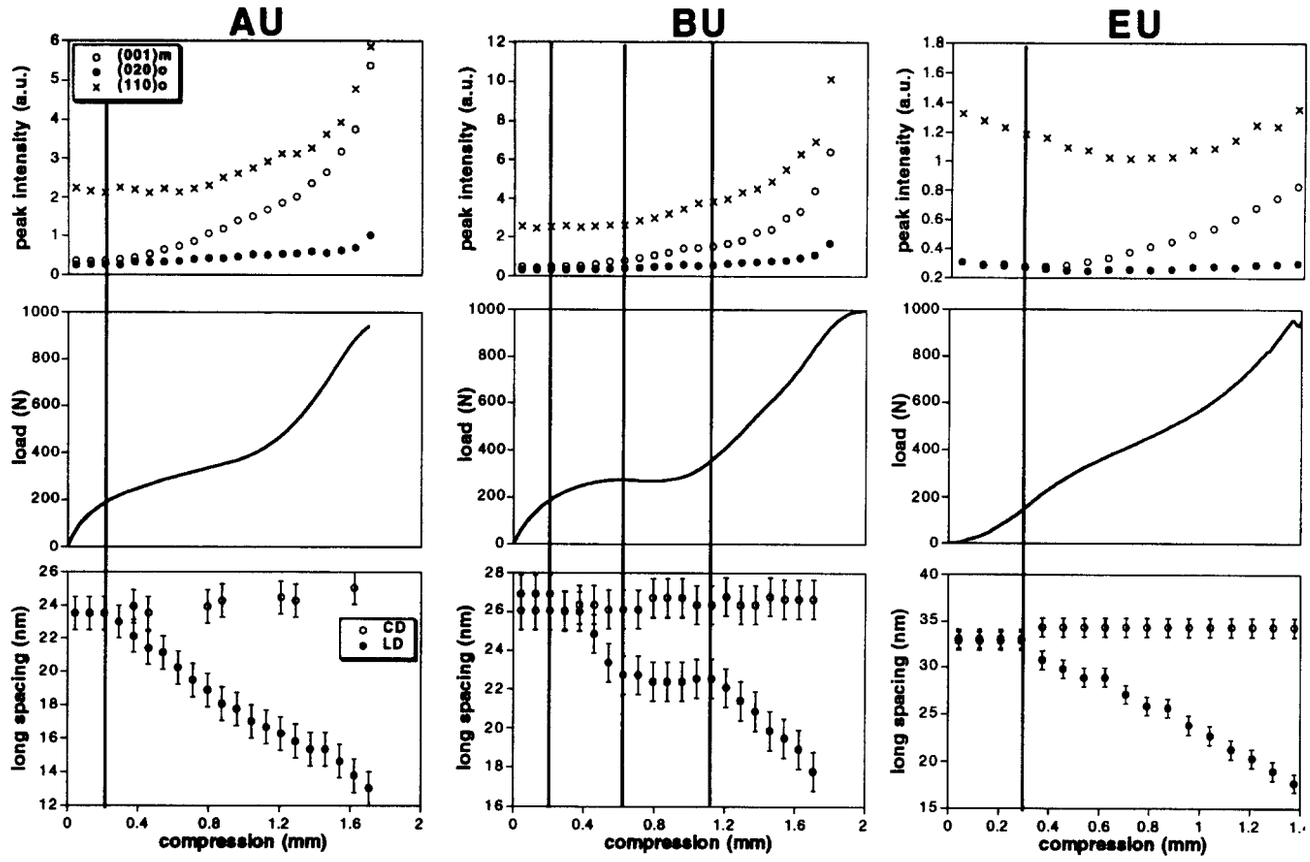

Figure 7 Correlation between the SAXS long spacings, WAXS peak intensities and load–compression curves for unannealed HDPE samples A and B and annealed HMW-HDPE sample E

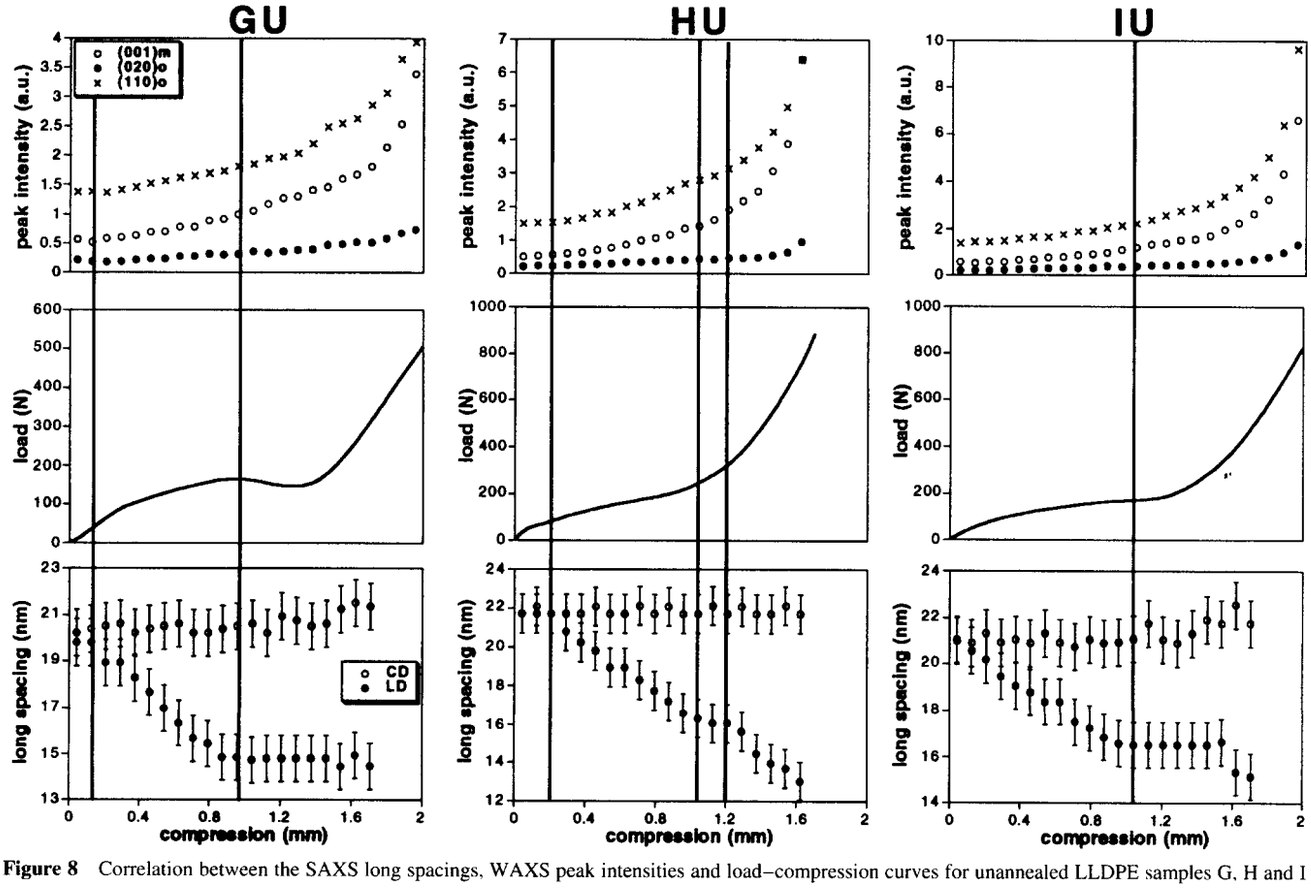

Figure 8 Correlation between the SAXS long spacings, WAXS peak intensities and load–compression curves for unannealed LLDPE samples G, H and I

any of the peak intensities during the very first stages of elastic deformation. At the yield point on the stress–strain curves (see *Figure 9*) the peak intensities and orientations began to change. The orthorhombic (110) and (020) reflections became oriented parallel to CD, and their intensity in this direction rose. The orthorhombic (200) reflection became much weaker parallel to CD and oriented towards LD. Less molecular orientation was attained in compression than in tension, however, and all of the reflections remained as arcs (see *Figures 3, and 5*). Untreated E differed from the other samples in that the orthorhombic (110) peak intensity decreased from the start of compression (see *Figure 7*), although it increased at higher strains, as for the other samples. The orientational sequence followed by the WAXS reflections in EU was also the same as for the other samples.

The monoclinic phase was detected in all of the samples at the yield point on the stress–strain curves (AU, BU and ESC) and during the yielding region of the load–compression curves (LLDPE samples), via the presence of the monoclinic (001) (see *Figures 7–9*), (020), (210) and ($\bar{2}$ 01) reflections. These reflections are indicated in *Figures 3 and 4*. As in the tensile specimens the monoclinic phase was oriented upon formation, with the (001) and (210) reflections initially aligned parallel to CD and the (020) and ($\bar{2}$ 01) reflections aligned parallel to LD. During compression the monoclinic phase became increasingly aligned. The (001) and (210) reflections remained parallel to CD and became more oriented and more intense whereas the (020) and ($\bar{2}$ 01) reflections moved away from LD towards CD via the formation of four point patterns. *Figure 6* clearly shows the increase in intensity of the monoclinic (001) reflection. The monoclinic (020) reflection overwhelmed the orthorhombic (200) reflection, and the resolution of the detector was insufficient to separate the two, rendering quantitative analysis of these reflections impossible after yield. The monoclinic reflections were less intense and occurred at higher strains in the LLDPE.

Small-angle X-ray scattering

The HDPE and LLDPE behaved similarly. During compression the initially isotropic SAXS pattern became oriented, and the scattering was concentrated in the direction parallel to LD, as can be seen in *Figures 3–5*. Comparison of the scattering patterns with the same frame numbers in *Figures 3, and 5*, which were taken at the same compressions, shows that the LLDPE was more oriented at a given compression. In *Figure 3* it can be seen that for HDPE the initially circular SAXS pattern became elliptical, with the longer axis parallel to LD, before the scattering assumed a two point shape with the intensity concentrated parallel to LD. *Figure 5* shows that the SAXS pattern for LLDPE, on the other hand, remained elliptical over a smaller deformation range before a discontinuous change to two discrete spots. At the largest compression achieved (a nominal compression of 2.0 mm) there was a difference between the HDPE and LLDPE. *Figure 10* shows the SAXS patterns at this compression for untreated HDPE and LLDPE samples. It can be seen that the LLDPEs had attained a two point spot like pattern (most noticeable for sample H) at this compression whereas the SAXS patterns for the HDPE samples, although definitely concentrated parallel to LD, retained a more elliptical character which is most clearly seen in the lowest molecular weight sample, A. Unlike tensile deformation, there were no signs of cavitation in HDPE compressed at room temperature.

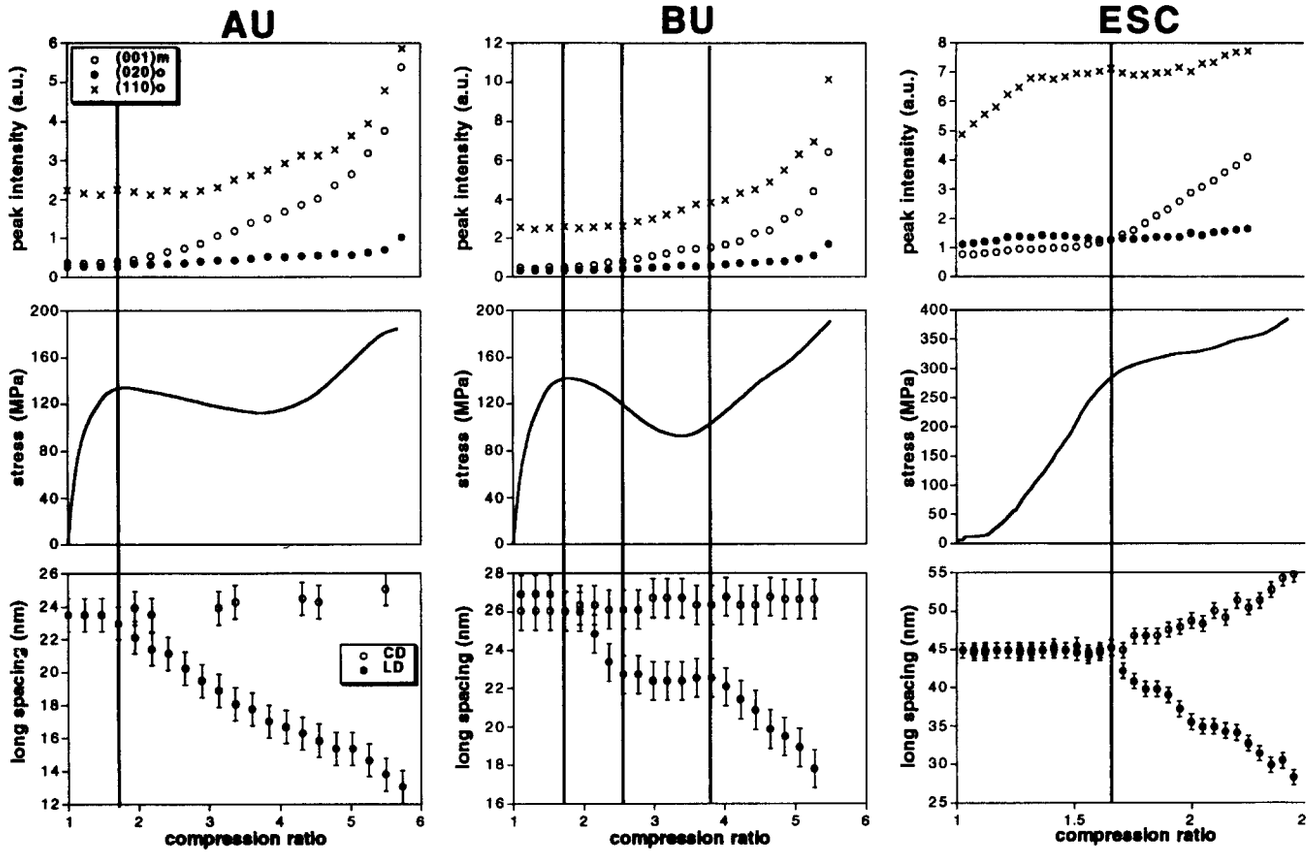

Figure 9 Correlation between the SAXS long spacings, WAXS peak intensities and stress–strain curves for unannealed HDPE samples A and B and annealed HMW-HDPE sample E

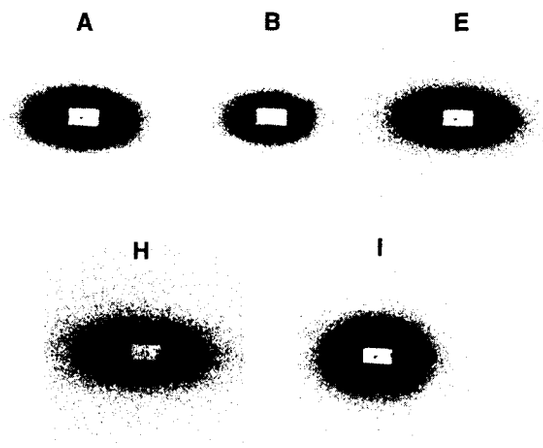

Figure 10 SAXS patterns measured at a compression of 2.0 mm, for HDPE, HMW-HDPE and LLDPE samples

Table 2 Compression at which L_{LD} began to decrease (e_L), the martensitic transformation became active (e_M) and the yield strain (e_y) for HDPE samples A and B

Sample	$e_L \pm 0.042$ (mm)	$e_{MT} \pm 0.042$ (mm)	e_y (mm)
A	0.208	0.292	0.333
B	0.208	0.292	0.333
E (unannealed)	0.292	0.375	–
E (annealed)	0.875	0.875	–
G	0.125	0.375	–
H	0.208	0.375	–
I	0.042	0.375	–

Table 3 Percentage reduction of L_{LD} for the samples compressed at 0.5 mm min^{-1} (top row) and 0.05 mm min^{-1} (bottom row)

HDPE			LLDPE		
A	B	E	G	H	I
41.3	29.7	29.4	22.7	30.8	27.0
–	–	19.5	19.0	20.8	–

The main quantitative feature from the SAXS was the correlation of the changes in long spacing measured parallel to LD (hereafter referred to as L_{LD}) with the load–compression (see *Figures 7 and 8*) and the stress–strain curves (see *Figure 9*). In all cases L_{LD} initially remained constant during the early stages of elastic deformation. It began to decrease before the yield point of the stress–strain curve. In the HDPEs the decrease occurred just prior to the activation of the martensitic transformation and noticeable changes in intensity and orientation of the orthorhombic reflections, whereas in the HMW-HDPE and LLDPE the decrease definitely preceded the martensitic transformation. *Table 2* records the compressions at which the onset of the reduction in L_{LD} was observed, along with the martensitic transformation onset and the yield strain (for AU and BU). The onset of the decrease of L_{LD} generally occurred at a lower strain in the LLDPE samples, occurring at the lowest strain in the least crystalline sample, I. L_{LD} continued to decrease throughout deformation for all samples. For samples B, E, G and H the decrease either slowed or halted in the yielding region of the load–compression and stress–strain curves. The onset of strain hardening coincided with a renewed decrease in L_{LD}. *Table 3* shows the percentage decrease in L_{LD} after a compression of 1.67 mm. With the exception of sample A, which showed a much larger decrease, the HDPE, HMW-HDPE and LLDPE samples drawn at the same strain rates gave similar values (although this differed depending on whether the samples had been annealed or not). Note, however, the uncertainty mentioned earlier regarding whether all of the samples will have deformed by the same amount.

During deformation the SAXS intensity profile parallel to LD changed markedly. *Figure 11* shows the SAXS intensity profiles measured parallel to LD and CD for HDPE B and LLDPE I. As well as an increase in intensity, resulting from the concentration of the scattering parallel to LD, an increase in scattering at higher angles was recorded for both HDPE and LLDPE. A general, although quite small, increase of the long spacing parallel to CD (L_{CD}) was detected, shown in *Figures 7–9*, beginning around the same strain at which L_{LD} began to decrease. It increased by a greater amount for ESC compared to EU. The increase continued throughout deformation.

Figure 12 shows the effect of compression rate on the long spacings of EU and HU. For both samples there was little difference between specimens compressed at 0.05 mm min^{-1} and 0.5 mm min^{-1}, although *Table 3* shows that the percentage reduction in L_{LD} was lower for the samples compressed at the lower rate for HMW-HDPE and LLDPE. However, for the specimens compressed at the fastest rate of 5.0 mm min^{-1} L_{LD} began to decrease at higher compression ratios, most noticeable in sample G, although it reached the same value obtained in the other specimens at a compression ratio between 2.0 and 2.5. No noticeable differences were observed for L_{CD} however, which increased in both cases.

DISCUSSION

Overview

The structural changes in compression are more complex than those in tension, and the data that can be obtained in real time is insufficient to elucidate completely the mechanisms active in compression and the complete texture of the deformed material. This is because scattering information can only be obtained from the LD–CD plane whereas the molecular orientation occurs parallel to FD, which is parallel to the X-ray beam. Therefore, information from the structure in the FD–LD and FD–CD planes cannot be obtained. It must be considered that the scattering patterns represent just one section through a potentially complex three-dimensional pattern in reciprocal space and that the changes in long spacing observed may be 'apparent' rather than 'real', i.e. the maxima may be a cut through the lateral part of the tails of the periodicity in another direction for which information is not obtainable from this study. Previous structural studies performed on unoriented PE[5–7] have mainly been performed *ex situ* and have utilised information from all of the above planes to determine the deformation mechanisms and the overall texture. Nevertheless, bearing the above argument in mind, the available information in this study can be used to draw some useful conclusions.

It should be noted that these results have demonstrated the necessity of calculating the stress–strain curve, since a precise macroscopic yield point could only be identified

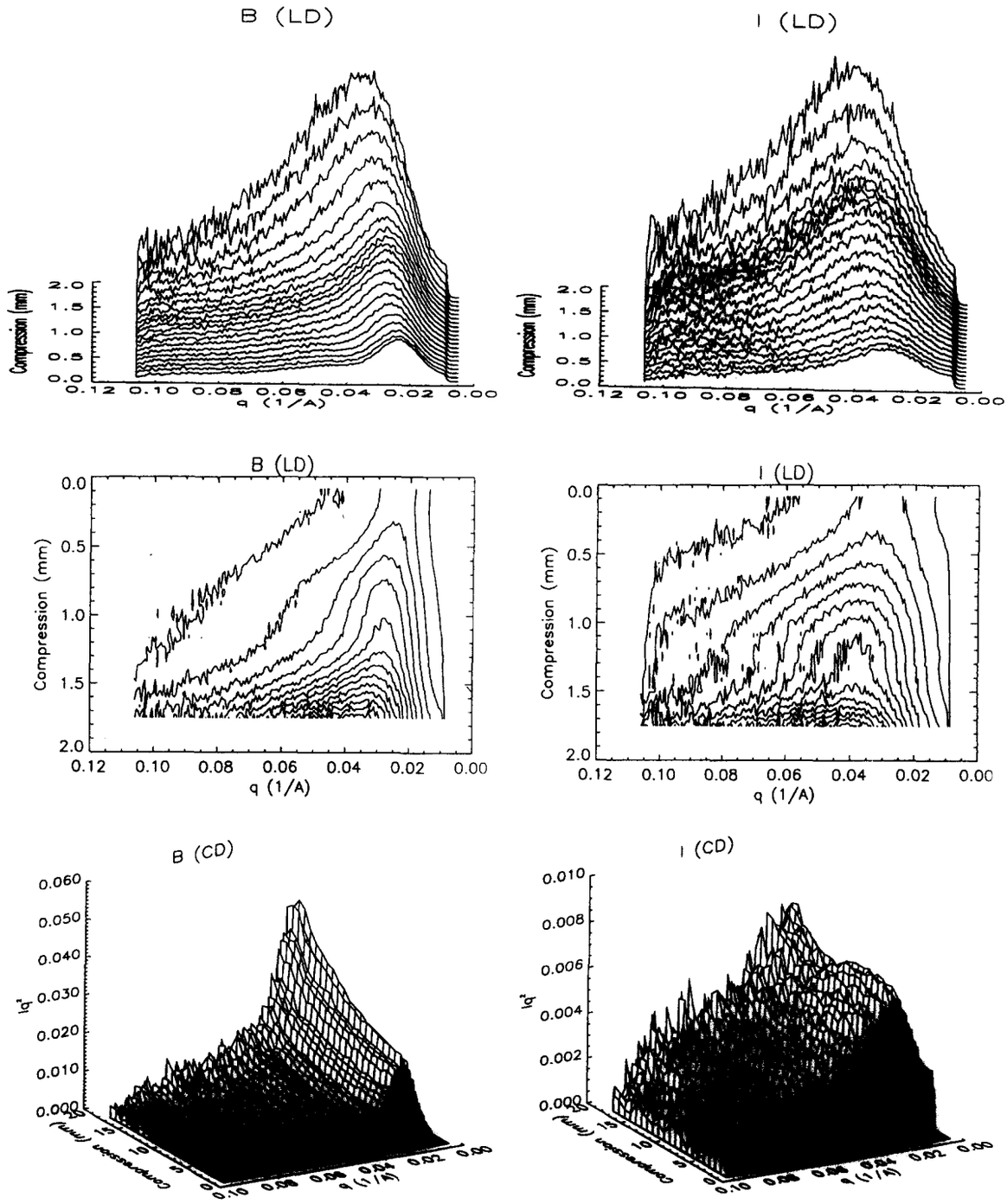

Figure 11 (a) SAXS intensity profiles and intensity contour plots parallel to LD comparing HDPE (sample B) with LLDPE (sample I). (b) SAXS intensity profiles parallel to CD comparing the same HDPE and LLDPE samples

in the stress–strain, not the load–compression, curves. Correlation of the macroscopic and microscopic deformation was therefore most effective for HDPE samples, in which a macroscopic yield point was identified.

Uniaxial compression deformation mechanism

The initially constant WAXS intensities and long spacings measured from SAXS suggest that, as for tensile deformation[1,2], elastic deformation proceeds with little or no drastic structural change. Interlamellar deformation modes, including interlamellar shear and lamellar rotation, can adequately explain the observed results.

It is recalled that, in tension, crystallographic deformation mechanisms suddenly became active at the yield point[1–3]. In compression, crystallographic deformation also occurred during macroscopic yielding, since the martensitic transformation and orientation of the orthorhombic reflections coincided with the yield point on the stress–strain curve. The onset of the decrease in L_{LD} at the yield point in tension was apportioned to the activation of chain slip[1,2]. In compression, the change in orientation of the orthorhombic reflections suggest that it is also likely that chain slip was activated at, and was responsible (at least partially) for, the reduction of the value of L_{LD} at the yield point. The

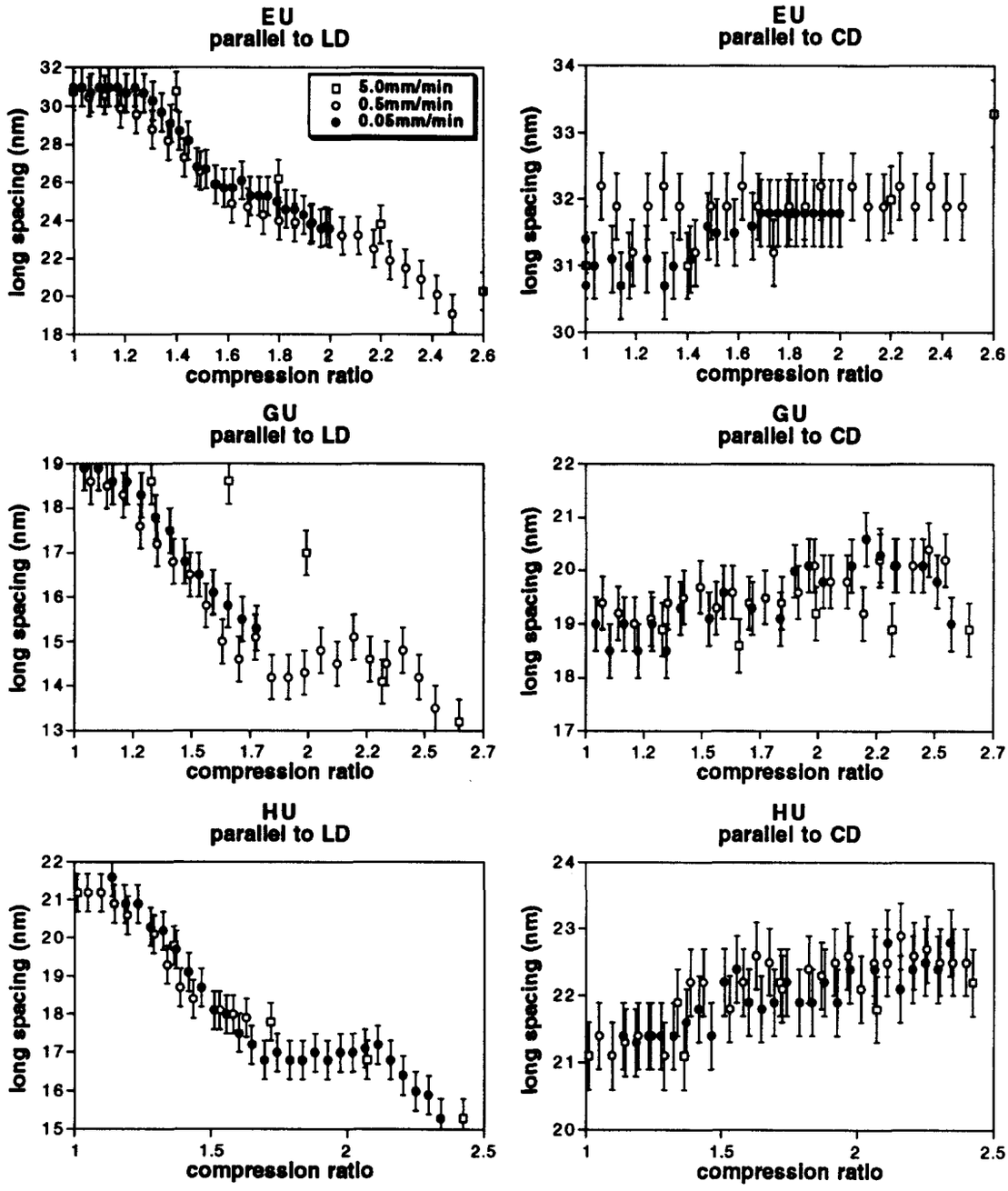

Figure 12 Effect of compression rate on the long spacings parallel to LD and parallel to CD for HMW-HDPE and LLDPE

activation of chain slip at the yield point corresponding with lamellar thinning has indeed been recorded previously for compressed HDPE[5] (although thinning of the amorphous component was also observed in this study, the reduction in long spacing was mainly due to lamellar thinning). However, a further mechanism is required to explain the reduction in L_{LD} prior to yielding. If the reduction in L_{LD} was solely caused by lamellar thinning due to chain slip, then the results would appear to confirm that chain slip was activated in preference to the martensitic transformation. Such an observation would accord with experimental evidence giving chain slip a lower CRSS[14,15]. However, it seems odd that the yield point should correspond to different mechanisms in tension and compression. Therefore, in order to comply with the reasoning used to explain the results of tensile deformation, a mechanism involving the inter-lamellar regions must be invoked to explain the reduction in L_{LD} before the yield point.

Following the logic applied in parts 1 and 2 of this series[1,2], crystallographic deformation should begin at higher strains in the less crystalline HMW-HDPE and LLDPE. Although the martensitic transformation complied with this reasoning, occurring at higher strains in the LLDPE and HMW-HDPE, the reduction in L_{LD} behaved oppositely. This observation may be explained if an interlamellar deformation process can also cause a L_{LD} to decrease. A candidate is simultaneous shear and rotation, depicted in *Figure 13*. Interlamellar sliding before chain slip has previously been observed in compression for HDPE[6]. If such a mechanism operated then the LLDPE and HMW-HDPE would indeed be expected to exhibit the reduction of L_{LD} at lower strains than in the HDPE, and L_{LD} could decrease prior to the yield point and the definite occurrence of crystallographic deformation without compromising the rationale adopted in explaining tensile deformation. Rotation and shear of lamellae will thus occur until the lamellae

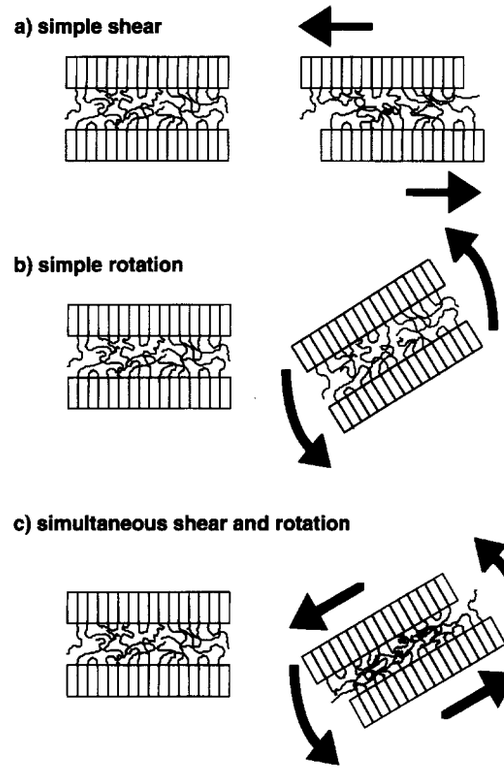

Figure 13 Schematic representation of (a) simple shear and (b) simple rotation of lamellae, indicating how the long spacing remains constant and (c) simultaneous shear and rotation of lamellar, showing how the long spacing decreases

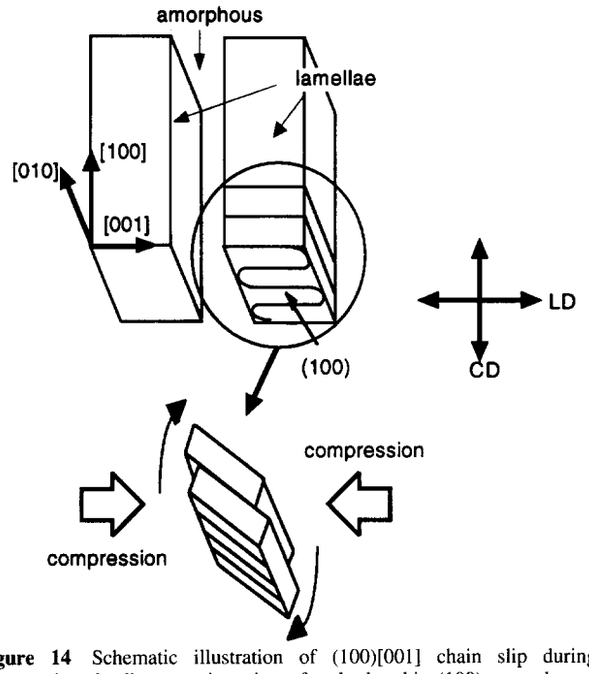

Figure 14 Schematic illustration of (100)[001] chain slip during compression, leading to orientation of orthorhombic (100) normals and lamellar normals parallel to the compression axis, and lamellar thinning

become sufficiently stressed for the chains to slip through them, i.e. once the CRSS for chain slip is reached.

The operation of simultaneous interlamellar shear and rotation at lower strains in the less crystalline LLDPE samples shows that in compression, as in tension, the interlamellar deformation mechanisms play a greater role in the less crystalline LLDPE samples. The more complete

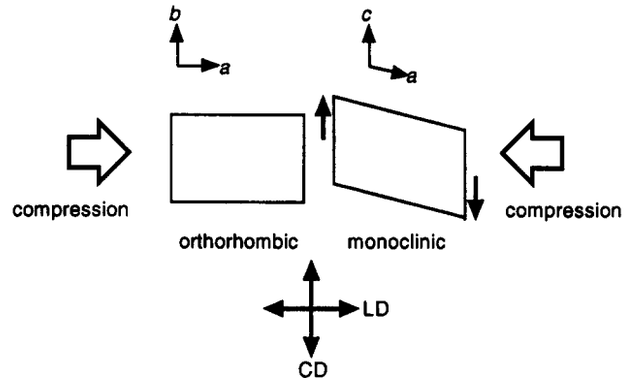

Figure 15 $T2_2$ martensitic transformation, showing a means of shear of the orthorhombic unit cell to a monoclinic one, with relation to the compression axis (LD)

lamellar reorientation that was observed in the LLDPEs provides further evidence for the increased role of the amorphous component in these samples. The elliptical nature of the SAXS patterns at high compressions for the HDPE samples implied that there was a greater range of lamellar orientations in these samples than in the LLDPEs, with their spot-like SAXS patterns. A larger amount of compliant amorphous material aids the reorientation of the lamellae by allowing them more freedom to comply with the applied deformation, presumably by means of inter-lamellar shear, rotation or both.

Some indications about the chain slip mechanism are provided by the observation that the orthorhombic (020) reflection became increasingly oriented parallel to CD while the orthorhombic (200) reflection and the lamellar normals became increasingly aligned parallel to LD. The operation of (100)[001] chain slip and (100)[010] transverse slip, shown in *Figure 14*, can explain these changes. As mentioned previously, where it was implicated in tensile deformation[1,2], (100)[001] chain slip has the lowest CRSS of the crystallographic deformation mechanisms, and therefore it is expected to be the dominant slip mode. It has also been positively identified in other compression studies of initially unoriented bulk HDPE[6,7], as well as in oriented HDPE[11]. There is no evidence for the activation of slip systems involving the (010) or (110) planes, since these would induce orientation of these planes towards LD. It has been suggested that the operation of lamellar shear may also play a part in the observed orientations of the reflections, a possibility which has some experimental support for the LLDPEs and cannot be discounted for the HDPEs[5]. That the initial orientation of the monoclinic reflections was the same as found in tensile deformation, but rotated by 90°, suggests that the martensitic transformation occurred in lamellae oriented with their normals parallel to LD. Lamellae in this orientation will be least inclined to deform by chain slip. From the initial orientation of the monoclinic reflections the $T2_2$ mode, which was postulated as the operative mode in tension[3], is a likely candidate as the operative transformation mode, via shear of the orthorhombic unit cell as schematically shown in *Figure 15*. Therefore, as with tensile deformation, the martensitic transformation occurs predominantly in regions where chain slip cannot operate. Increasing orientation of the monoclinic phase during compression explains the observed changes in position of the monoclinic reflections.

The activation of the martensitic transformation at higher strains in the LLDPE and HMW-HDPE compared to the

HDPE can be explained by the greater amount of amorphous material bearing a greater amount of deformation in the former two materials, thus delaying the onset of crystallographic deformation to higher strains.

The reason for the change in rate of decrease of L_{LD} after the yield point cannot be ascertained with certainty without structural information from the LD–FD and CD–FD planes. However, a possible reason may be speculated upon. A study of HDPE, using SAXS and TEM, has indicated that at a compression ratio of 3.13, lamellae begin to fragment in a re-structuring process that leads to the formation of a new long spacing measured in the LD–FD plane[6]. Fragmentation at a critical strain during compression has also been observed in a separate study[5]. It is likely that molecular weight and thermal history will alter the precise strain at which this process occurs, so the value of the compression ratio at which L_{LD} stopped decreasing in BU, which was 2.57, need not be regarded as too dissimilar to 3.13. Lamellar fragments formed during the re-structuring process could have caused the increase in SAXS at higher angles and widening of the SAXS profiles parallel to LD. The absence of cavitation in the HDPE during lamellar disintegration can be explained by the large pressure component in the deformation[6]. Owing to the compliance of the amorphous component, once the lamellae have fragmented, their remains may rotate easily without further structural change and without producing any additional strain. This effect may be responsible for the smaller rate of decrease of L_{LD} during strain softening, since the reduction of chain slip during rotation would reduce the amount of lamellar thinning. Following the reorganisation, deformation of the amorphous component would become increasingly difficult, causing strain hardening as interlamellar chains extended. Major lamellar deformation would recommence as the extending amorphous material pulled chains through the reoriented lamellae. Thinning of these lamellae, as chain slip proceeded, would then cause a further reduction of the long spacing parallel to LD. That the renewed reduction in the LLDPE samples either began at a higher strain (sample I, *Figure 8*) than for the HDPE of similar molecular weight (sample B, *Figure 7*) or did not show a further reduction in long spacing parallel to LD (sample G, *Figure 8*), possibly resulted from the short chain branches in LLDPE inhibiting the slippage of chains through the reoriented lamellae (the behaviour of LLDPE sample H is the exception, and may possibly be related to the heterogeneous branch distribution in this sample). The smaller percentage decrease in L_{LD} for the LLDPEs is also consistent with the notion of an increased contribution to the deformation from the amorphous component in these samples. The much larger decrease in L_{LD} for sample A compared to the other HDPEs and LLDPEs may be related to the lower molecular weight of this sample enabling chain slip, leading to lamellar fragmentation and possibly decrystallisation, to occur to a greater extent.

The increase in the value of L_{CD} occurs because the lamellae with normals parallel to CD experience an extensional stress. It is expected that this would cause them to separate affinely undergoing no structural change, which explains the constant SAXS intensity profile parallel to CD for these samples. The onset of the increase at a lower strain for the untreated compared to the annealed HMW-HDPE probably results from the increased compliance due to the greater amount of amorphous material in the untreated sample. The reason for the onset of lamellar separation parallel to LD at the same strain at which the martensitic transformation and chain slip occurred, seen most definitely in *Figure 8* for the annealed HMW-HDPE, is uncertain. Interlamellar separation is expected to occur during elastic deformation since it results from deformation of the amorphous component. Perhaps the onset of chain slip coincides with the release of constraints which enable the lamellae parallel to LD to separate. Unfortunately, owing to the slowness of the change, neither the strains at which the increase began nor the rates of increase for the untreated samples could be precisely ascertained, thus preventing comparison of untreated HDPE and LLDPE.

So far, the influence of branch type has not been mentioned. The results show that, as for tensile deformation, the percentage crystallinity rather than branch type was most probably responsible for the observed differences between the LLDPEs. Increasing ease of simultaneous shear and rotation with decreasing crystallinity explains the decrease in L_{LD} at lower strains in the less crystalline samples. Mostly, the results emphasise the similarity between the different LLDPE samples.

The influence of molecular weight has also been explained in terms of its influence on the percentage crystallinity. Nevertheless, there were notable differences between EU, ESC and the HDPE samples A and B, which could not be explained in this way. The initial decrease in orthorhombic (110) intensity in EU and its subsequent increase is explicable in terms of the combined influences of the obstruction of the incident beam by one of the compression dies and the increasing orientation of the (110) reflection parallel to CD. ESC presents another uncertainty, and the reason for the initial increase of the orthorhombic (110) intensity parallel to CD during elastic deformation (see *Figure 9*) remains unexplained. The much larger values of the compression at which the martensitic transformation and reduction in L_{LD} was recorded for ESC (see *Table 2*) are believed to be inaccurate due to the unreliability in compression values given by the Minimat (see earlier) compounded with the fact that the results from ESC were recorded on a different occasion to the untreated samples using different apparatus. The results from ESC are included mainly for comparison of the SAXS, WAXS and stress–strain curve rather than for comparison with the other samples.

The influence of compression rate

As the compression rate increases the system has a shorter time to respond to the deformation. Some disentanglement of chains in the amorphous component is necessary during plastic deformation. The long spacing remains constant to higher compression ratios because the chains are unable to disentangle sufficiently to allow shear and rotation. However, because the microstructure must comply with the externally imposed deformation the lamellar deformation at high compression ratios is independent of compression rate. At yield, which has been identified with chain slip, the long spacing does begin to decrease at the higher compression rate. This suggests that once flow begins the lamellae fail rapidly, accommodating the deformation that the amorphous component was unable to at earlier stages of deformation.

CONCLUSIONS

In compression, as in tension, HDPE, HMW-HDPE and LLDPE behaved in a similar manner, and their differences could explained in terms of the different amounts of

amorphous material possessed by each type of PE. A similar sequence of textural changes to those found in tensile deformation were proposed to occur which accounted for the observed shape of the stress–strain curve. Structural changes were less drastic in compression, however, and the widespread cavitation that occurred at the onset of lamellar fragmentation during cold-drawing of HDPE was completely absent when the lamellae fragmented in compression.

Elastic deformation corresponded to deformation mechanisms involving the amorphous component, such as interlamellar shear and/or rotation. A simultaneous lamellar shear and rotation process was proposed to operate before yield, becoming more dominant with decreasing percentage crystallinity. As for tensile deformation, the yield point in the stress–strain curve during compression corresponded to the activation of crystallographic deformation mechanisms, namely chain slip and a martensitic transformation. It is likely that the chain slip mode was the (100)[001]mode. The martensitic transformation was supplementary to chain slip, occurring in regions of the structure where chain slip was unfavoured, i.e. lamellae with normals parallel to the compressive axis, and could be explained by the operation of the $T2_2$ mode.

Upon yielding the lamellae oriented, by means of interlamellar mechanisms and chain slip, so that their normals became aligned parallel to the compression axis. At a certain strain after yielding, however, they began to fragment and the fragments rotated so that the chain axis could align parallel to the flow direction, perpendicular to the compressive axis. Rotation was followed by the further operation of crystallographic deformation mechanisms, once the amorphous component was unable to deform further, causing continued lamellar thinning and strain hardening.

As found during tensile deformation, the amount of compliant amorphous material was important in aiding the process of rotation and disruption of lamellae. The greater the amount of amorphous material the easier it was for the lamellae to reorient, leading to a greater degree of lamellar orientation in the less crystalline LLDPE samples. However, the short chain branches in the LLDPE samples inhibited the ease of chain slip following lamellar reorientation in these samples and caused the crystallographic deformation mechanisms to occur at higher strains in the reoriented structure.

Differences between the LLDPE types were minimal, and were explicable in terms of percentage crystallinity rather than branch type. In compression, as well as in tension, branch length had a negligible influence on the mechanical behaviour of PE.

ACKNOWLEDGEMENTS

The help of the following people is gratefully acknowledged: Dr. Elinor Kerr, of BP Chemicals, Mary Vickers, of the Department of Materials Science and Metallurgy, University of Cambridge, Pete Bone and Lara Stoimenof, of the Cavendish Laboratory, University of Cambridge, and Mary Heppenstall-Butler, of UMIST. We are indebted to staff at the CCLRC Daresbury Laboratory, including Elizabeth Towns-Andrews, Geoff Mant and Anthony Gleeson, for their technical support which enabled these experiments to be perfomed and for the provision of programs from the CCP13 software suite which were employed in the data analysis. The financial support of the EPSRC and BP Chemicals is acknowledged.

REFERENCES

1. Butler, M. F., Donald, A. M. and Ryan, A. J., *Polymer*, 1997, **38**, 5521.
2. Butler, M. F., Donald, A. M. and Ryan, A. J., *Polymer*, accepted.
3. Butler, M. F., Donald, A. M., Bras, W., Mant, G. R., Derbyshire, G. E. and Ryan, A. J., *Macromolecules*, 1995, **28**, 6383.
4. Grubb, D. T. and Prasad, K., *Macromolecules*, 1992, **25**, 4575.
5. Bartzcak, Z., Cohen, R. E. and Argon, A. S., *Macromolecules*, 1992, **25**, 4692.
6. Galeski, A., Bartzcak, Z., Argon, A. S. and Cohen, R. E., *Macromolecules*, 1992, **25**, 5705.
7. Krause, S. J. and Hosford, W. F., *J. Polym. Sci., Polym. Phys. Edn.*, 1989, **27**, 1853.
8. Keller, A. and Rider, J. G., *J. Mater. Sci.*, 1966, **1**, 389.
9. Cowking, A. and Rider, J. G., *J. Mater. Sci.*, 1969, **4**, 1051.
10. Keller, A. and Pope, D. P., *J. Mater. Sci.*, 1971, **6**, 453.
11. Young, R. J., Bowden, P. B., Ritchie, J. M. and Rider, J. G., *J. Mater. Sci.*, 1973, **8**, 23.
12. Shinozaki, D. M. and Groves, G. W., *J. Mater. Sci.*, 1973, **8**, 1012.
13. Pope, D. P. and Keller, A., *J. Polym. Sci., Polym. Phys.*, 1975, **13**, 533.
14. Bowden, P. B. and Young, R. J., *J. Mater. Sci.*, 1975, **9**, 2034.
15. Lin, L. and Argon, A. S., *J. Mater. Sci.*, 1994, **29**, 294.
16. Bartzcak, Z., Argon, A. S. and Cohen, R. E., *Macromolecules*, 1992, **25**, 5036.
17. Peterlin, A., *J. Mater. Sci.*, 1971, **6**, 490.
18. Young, R. J., *Philos. Mag.*, 1974, **30**, 85.
19. Shadrake, L. G. and Guiu, F., *Philos. Mag.*, 1976, **34**, 565.
20. Young, R. J., *Mater. Forum*, 1988, **11**, 210.
21. Crist, B., Fischer, C. J. and Howard, P. R., *Macromolecules*, 1989, **22**, 1709.
22. Flory, P. J. and Yoon, D. Y., *Nature*, 1978, **272**, 226.
23. Wignall, G. D. and Wu, W., *Polym. Commun.*, 1983, **24**, 534.
24. Hendra, P. J., Taylor, M. A. and Willis, H. A., *Polymer*, 1985, **26**, 1501.
25. Phillips, P. J. and Philpot, R. J., *Polym. Commun.*, 1986, **27**, 307.
26. Liu, T. and Harrison, I. R., *Polymer*, 1987, **28**, 1861.
27. Zhan, C.-M., *J. Macromol. Sci.-Phys.*, 1991, **30**, 63.
28. Wu, W., Wignall, G. D. and Mandelkern, L., *Polymer*, 1992, **33**, 4137.
29. Butler, M. F., Ph.D. Thesis, University of Cambridge, UK, 1996.
30. Towns-Andrews, E., Berry, A., Bordas, J., Mant, G. R., Murray, P. K., Roberts, K., Sumner, I., Worgan, J. S., Lewis, R. A. and Gabriel, A., *Rev. Sci. Instrum.*, 1989, **60**, 2346.
31. Bliss, N., Bordas, J., Fell, B. D., Harris, N. W., Helsby, W. I., Mant, G. R., Smith, W. and Towns-Andrews, E., *Rev. Sci. Instrum.*, 1995, **66**, 1311.
32. Bilsborrow, R. L., Bliss, N., Bordas, J., Cernik, R. J., Clark, G. F., Clark, S. M., Collins, S. P., Dobson, B. R., Fell, B. D., Grant, A. F., Harris, N. W., Helsby, W. I., Smith, W. and Towns-Andrews, E., *Rev. Sci. Instrum.*, 1995, **66**, 1633.